Surface growth approach for bulk reconstruction in the AdS/BCFT correspondence*

Xi-Hao Fang (方西浩)† Fang-Zhong Chen (陈方中)‡ Jia-Rui Sun (孙佳睿)§

School of Physics and Astronomy, Sun Yat-Sen University, Guangzhou 510275, China

Abstract: In this study, we extend the surface growth approach for bulk reconstruction into the AdS spacetime with a boundary in the AdS/BCFT correspondence. We show that the geometry in the entanglement wedge with a boundary can be constructed from the direct growth of bulk extremal surfaces layer by layer. Furthermore, we observe that the surface growth configuration in BCFT can be connected with the defect multi scale entanglement renormalization ansatz (MERA) tensor network. Additionally, we investigate the entanglement of purification within the surface growth process, which not only reveals more refined structure of entanglement entropy in the entanglement wedge but also suggests a selection rule for surface growth in the bulk reconstruction.

Keywords: AdS/CFT correspondence, gauge/gravity duality, models of quantum gravity

DOI: 10.1088/1674-1137/ad32be

I. INTRODUCTION

There are different approaches in finding the quantum theory of gravity. One of the most promising approaches is the AdS/CFT correspondence or gauge/gravity duality developed from string theory. The AdS/CFT correspondence reveals that an n-dimensional gravitational system in the bulk asymptotically AdS spacetime is equivalent to an $(n-1)$-dimensional CFT on the timelike AdS boundary [1−3]. This provides new perspectives and powerful tools to study strongly coupled field theories as well as quantum gravity. One of the most important progresses in the study of the AdS/CFT correspondence is the holographic interpretation of the entanglement entropy, i.e., the entanglement entropy between subsystem A and its complement B in a boundary CFT can be denoted by the area A_γ of the minimal or extremal surface γ (which is homologous to the boundary ∂A) in the bulk AdS spacetime. This is termed as the Ryu-Takayanagi (RT) formula of the holographic entanglement entropy (HEE) [4−7]

$$S_A = \frac{A_\gamma}{4G_N}, \tag{1}$$

where G_N denotes the Newtonian constant. The formula in Eq. (1) establishes the connection between entanglement entropy of boundary quantum fields and geometry of bulk gravity, which has been shown to play a key role in the bulk reconstruction, namely, using the information of the operators in the boundary CFT to reconstruct the bulk AdS gravity [8−12]. This is just the emergent phenomenon of gravity indicated by the AdS/CFT correspondence and the broader gauge/gravity duality [1, 3]. An important progress in studying bulk reconstruction in holography is the introduction of a new approach from quantum manybody systems, termed as multi-scale entanglement renormalization ansatz (MERA) of tensor networks [13−16]. MERA was originally served as a method to reduce computational complexity in solving the Schrödinger equation of the lattice quantum manybody systems. It has been shown that the orientation of entanglement renormalization within MERA can be interpreted as the radial direction of the bulk AdS spacetime, which provides novel insights into the emergence of gravity and realization of AdS/CFT correspondence. Many different tensor networks have been studied to realize the models of holographic duality [17−20].

Recently, increasing evidence suggests a profound connection between quantum entanglement and the fundamental nature of spacetime geometry and gravity. Notable examples include the subregion-subregion duality in entanglement wedge reconstruction and the bulk reconstruction from boundary quantum error code [21−24]. An

Received 13 February 2024; Accepted 11 March 2024; Published online 12 March 2024

* Supported by the National Natural Science Foundation of China (11675272)

† E-mail: fangxh9@mail2.sysu.edu.cn

‡ E-mail: chenfzh7@mail2.sysu.edu.cn

§ E-mail: sunjiarui@mail.sysu.edu.cn

important question involves finding general and more efficient approaches to reconstruct bulk geometry and gravitational dynamics from the information of boundary operators. Very recently, a new method for bulk reconstruction, known as the surface growth approach, was proposed in [25, 26], as illustrated in Fig. 1. This scheme suggests that the bulk AdS spacetime can be constructed by layer-by-layer growth of bulk extremal surfaces from the boundary, analogous to Huygens' principle of wave propagation. It has been shown that the surface growth scheme can correspond to a MERA-like tensor network, termed as the one shot entanglement distillation (OSED) tensor network [17]. Furthermore, it has been explicitly realized by direct growth of bulk extremal surfaces in asymptotically AdS_3 spacetime [27].

On the other hand, when the boundary CFT contains additional spatial boundary, its holographic duality is a bulk asymptotically AdS spacetime with a brane in it, which is termed as the AdS/BCFT correspondence [28−31]. The BCFT introduces several novel properties when compared to the ordinary CFT, one significant aspect being that the entanglement entropy receives contributions from the boundary. According to the HEE description, the bulk extremal surface can terminate on both the AdS boundary and the brane within the bulk AdS spacetime [28, 29]. This provides a natural picture of boundary to bulk propagation and can be viewed as process of bulk reconstruction from entanglement entropy. Additionally, the AdS/BCFT correspondence has been used as an equivalent description for entanglement island in the braneworld viewpoint, see, for example [32−36]. It is therefore compelling to further explore entanglement entropy and bulk reconstruction in asymptotically AdS spacetimes with boundaries. In this study, we expand the surface growth approach for bulk reconstruction to the AdS/BCFT correspondence. We demonstrate how the entanglement wedge, with a boundary on the brane, can be effectively constructed through the growth of bulk extremal surfaces. We also discuss potential links between the surface growth configuration and defect MERA and defect OSED tensor networks. Furthermore, we analyze the entanglement of purification by examining the entanglement wedge cross section during the surface growth process. This analysis reveals the fine structure of entanglement entropy within the entanglement wedge and proposes a selection rule for surface growth in bulk reconstruction under the AdS/BCFT correspondence.

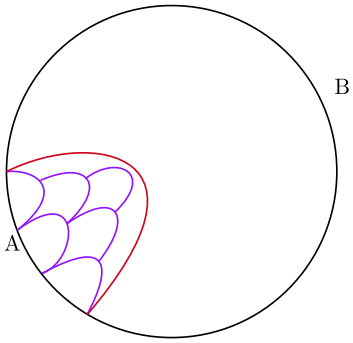

Fig. 1. (color online) Surface growth scheme in the AdS spacetime, bulk extremal surfaces growing from subintervals in subregion A provides an efficient way to construct the bulk geometry and detect the fine structure of entanglement entropy in the entanglement wedge.

This paper is organized as follows: In Sec. II, we briefly review of the HEE in the AdS/BCFT correspondence. In Sec. III and Sec. IV, we study the surface growth scheme in $AdS_5/BCFT_4$ correspondence, both in the homogeneous and inhomogeneous subregion cases, and discuss the connection between the surface growth configuration with the defect tensor network. In Sec. V, we study entanglement of purification in $AdS_3/BCFT_2$ by analyzing the entanglement wedge cross section in the surface growth process. Finally, we present our conclusions and discussion.

II. HEE IN THE ADS/BCFT CORRESPONDENCE

The AdS_{d+1} spacetime in Poincaré coordinates can be expressed by:

$$\mathrm{d}s^2 = \frac{L^2}{z^2}\left(-\mathrm{d}t^2 + \mathrm{d}z^2 + \mathrm{d}x_i\mathrm{d}x^i\right), \tag{2}$$

where $i = 1, 2, \ldots, d-1$ and L denotes the curvature radius. The asymptotically timelike boundary of the AdS spacetime is located at $z = \epsilon \to 0$. Considering the entanglement entropy of a strip-like subregion A with $x_1 \equiv x \in [-l/2, l/2]$, the bulk codimension-2 static minimal surface is $x = x(z)$, its explicit form is determined by the Euler-Lagrange equation for its area functional $A = L_0^{d-2}\int \frac{L^{d-1}}{z^{d-1}}\sqrt{1+x'^2}\mathrm{d}z$, which can be expressed as:

$$x' = \frac{1}{\sqrt{\frac{z_*^{2d-2}}{z^{2d-2}} - 1}}, \tag{3}$$

where it is assumed that x_a for $a = 2, 3, \ldots, d-2$ are in the box region with a length of L_0. The turning point of the bulk extremal surface is z_*, which satisfies $x'(z_*) = +\infty$ and

$$\int_0^{z_*} x'(z)\mathrm{d}z = \int_0^{z_*} \frac{\mathrm{d}z}{\sqrt{\frac{z_*^{2d-2}}{z^{2d-2}} - 1}} = \frac{l}{2}. \tag{4}$$

When choosing the background spacetime to be pure AdS_5 spacetime without boundary,

$$z_* = \frac{l\Gamma\left(\frac{1}{6}\right)}{2\sqrt{\pi}\Gamma\left(\frac{2}{3}\right)}. \tag{5}$$

The equation of the minimal surface γ is a hypergeometric function:

$$x = \frac{z_*}{4}\left(\frac{z}{z_*}\right)^4 F\left(\frac{1}{2},\frac{2}{3},\frac{3}{5},\left(\frac{z}{z_*}\right)^6\right). \tag{6}$$

When considering a bulk spacetime, which is a portion of the AdS spacetime, there is a boundary Q which can be regarded as a brane in the bulk spacetime. Based on the perspective of boundary CFT side, there is a spatial boundary P which is homologous to Q. This is termed as the BCFT. The existence of a boundary has nontrivial effects both on the gravity and CFT sides. In the case of a bulk minimal surface encountering a d dimensional brane Q, which can be regarded as the end-of-world (EOW) brane in the bulk AdS spacetime, and in the Poincaré coordinate, the location of a flat boundary (brane) can be determined by $x = z\tan\theta$, where $\theta+\pi/2$ is the angle between the brane and AdS boundary. For a strip-like bulk minimal surface γ intersecting with the boundary on point P_0 with coordinate $(z_0\tan\theta, z_0)$ in the (x,z) plane, the boundary condition requires that γ must be perpendicular to boundary Q. Hence, the unit normal vectors of the boundary $\hat{n}_Q$ should be perpendicular to the unit normal vectors of the minimal surface $\hat{n}_\gamma$ where $\hat{n}_Q\cdot\hat{n}_\gamma = 0$, which leads to $x'(z)|_Q = -\cot\theta$. By integrating the equation of motion with the boundary condition,

$$\int_\epsilon^{z_*} x'(z)\mathrm{d}z + \int_{z_*}^{z_0} x'(z)\mathrm{d}z = z_0\tan\theta + l, \tag{7}$$

the turning point z_* is obtained as:

$$\frac{l}{z_*} = \frac{2\sqrt{\pi}\Gamma(\frac{2}{3})}{\Gamma(\frac{1}{6})} + \frac{B\left(\cos^2\theta;\frac{2}{3},\frac{1}{2}\right)}{6} - \tan\theta(\cos\theta)^{1/3}, \tag{8}$$

in which subregion A is chosen as $x_1 \equiv x \in [-l, 0]$, $B(z,a,b)$ represents the incompatible Beta function, and ϵ denotes the UV cutoff of the BCFT. Subsequently, by further dividing coordinate x of the strip-like subregion A into multiple intervals, we can construct the surface growth from these subintervals layer-by-layer in subregion A.

III. SURFACE GROWTH SCHEME IN ADS$_5$ SPACETIME WITH BOUNDARY

To generalize the surface growth scheme into asymptotically AdS spacetime with boundary Q and observe how the presence of spatial boundary affects the configuration of growing minimal surfaces, first, let us consider a half-infinite strip boundary Q in the bulk AdS spacetime, where the boundary of the BCFT is located at $x = x_P$. The strip-like subsystem A is divided into several subintervals as $\{x_N, x_{N+1}\}$, $(N\in\mathbb{N})$, where each endpoint of the subinterval is the starting point of the bulk minimal surface $\gamma_N|_{z=\epsilon}$. Given the restriction imposed by boundary Q on the half strip, the bulk minimal surface corresponding to interval, which contains x_P, will end on (perpendicular to) brane Q. Therefore, naturally, the bulk minimal surfaces are classified into two types: type $\mathcal{A}$ surfaces, which intersect on boundary Q and have a vertical intersection, while type $\mathcal{B}$ surfaces have both endpoints attaching on boundary CFT, see Fig. 2.

After obtaining the first layer of bulk minimal surfaces in the strip-like subregion A, as shown in Fig. 2, one can further construct the geometry in a larger region in the entanglement wedge through the growth of bulk minimal surfaces. Following the approach in [26], in the same spirit of the Huygens' principle of wave propagation, one layer of bulk minimal surface on any cutoff surface in AdS spacetime can be viewed as the starting point for bulk minimal surfaces of the next layer. This provides the initial conditions for the Euler-Lagrange Eq. (3) satisfied by the bulk minimal surfaces. For example, considering two neighboring minimal surfaces γ_N and γ_{N+1} on two type $\mathcal{B}$ adjoining intervals $\{x_N, x_{N+1}\}, \{x_{N+1}, x_{N+2}\}$, respectively, it is possible to choose appropriate starting/ending points on each of them to determine the next layer of bulk minimal surfaces.

To fully construct the geometry in the entanglement wedge of subregion A with boundary from the growth of bulk minimal surfaces, additional starting/ending points on the boundary Q are necessary, separately from starting/ending points on the turning point z_* and the points on the bulk extremal surface of subregion A. This selection of bulk extremal surfaces guarantees continuity between the preceding and succeeding layers and also ensures the seamless propagation of information from the boundary CFT to the interior of bulk AdS spacetime. More explicitly, when dealing with a type $\mathcal{A}$ surface that intersects with the boundary, its effect extends to the next layer as long as it continues to intersect with the boundary. This leads to a situation where the initial condition of $x'(z)$ is determined by the turning point of the previous layer, z_*, and a point on the boundary Q, denoted as (x_0, z_0). The initial conditions are adopted to define the RT surface in the subsequent layer. Furthermore, apart from bulk minimal surfaces in the first layer, subsequent layers are no longer directly connected to the entanglement entropy of subregions in the boundary CFT. They instead reflect the manner in which the information of the boundary CFT will propagate into the deep AdS space-

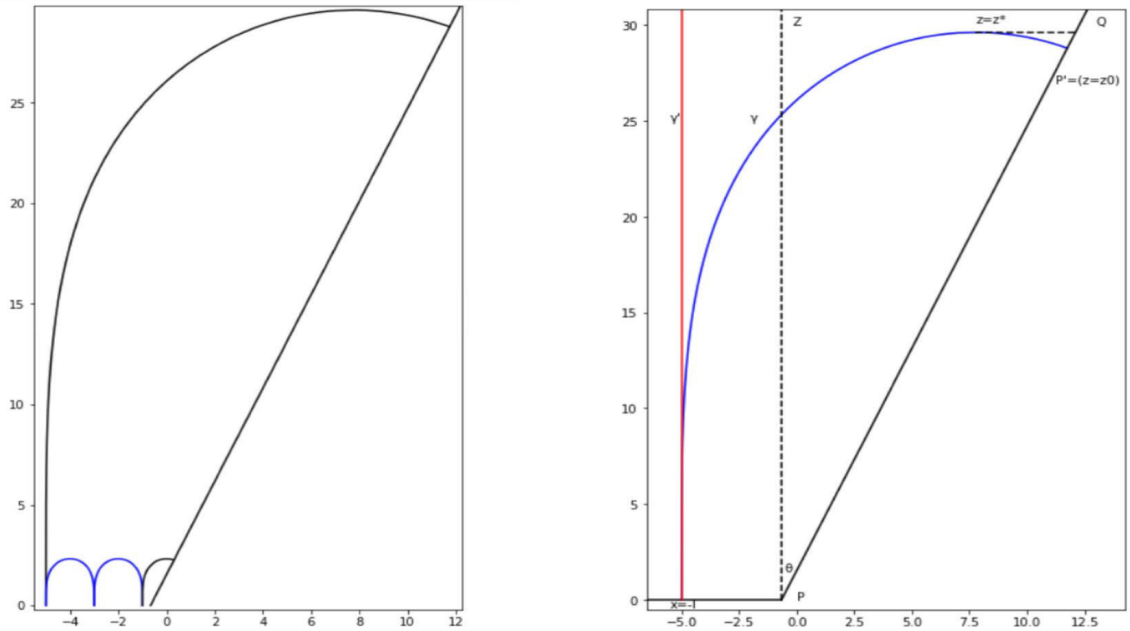

Fig. 2. (color online) Left: the first layer of strip-like bulk minimal surfaces in subregion A in the AdS_5 spacetime with boundary, $\theta=\frac{\pi}{4}$, the size of the left two subintervals in A is $\Delta x_1=2$, and the remaining subinterval is $\Delta x_1=0.18$, and $L=1$. The blue surface represents type $\mathcal{B}$ minimal surface, black surface represents the boundary (defect) type $\mathcal{A}$ minimal surface, which will end on the boundary. Right: the bulk minimal surface, which intersects with the boundary with vertical boundary condition, the blue line denotes type $\mathcal{A}$ minimal surface, the red line represents the asymptotic curve parallel to the z-axis, and subregion A is chosen as $x_1\in(-5,0)$. Both figures are drawn in x_1-z plane.

time. The bulk extremal surfaces are generalized RT surfaces denoted as $\bar{\gamma}$ and they provide a more refined description of entanglement entropy in subregion-subregion duality in the entanglement wedge reconstruction [26]. The surface growth scheme involves iterating this procedure layer-by-layer. Hence, eventually the entire entanglement wedge of the subregion A is filled. This provides a direct and efficient way to construct the bulk geometry in the entanglement wedge, as shown in Fig. 3.

It should be noted that in the presence of a boundary Q, the area of bulk extremal surface within each layer of surface growth does not exhibit a strictly decreasing trend solely with respect to the radial coordinate z, which is distinct with the monotonicity property in surface growth process without boundary, as depicted in the left and right figures of Fig. 4. The appearance of this new phenomenon is due to the boundary effect, namely, the existence of additional spatial boundary Q imposes constraints on the growth rules. This leads to a situation where surfaces within the same layer do not possess identical horizontal positions. Hence, this effect results in non-monotonic variations in surface area across layers. However, for regions near the apex of the outer entanglement wedge, the areas of growing extremal surfaces still exhibit a monotonically decreasing property, which is similar to the surface growth process without boundary. This new property highlights the important role of boundary conditions in shaping the spatial distribution of growing extremal

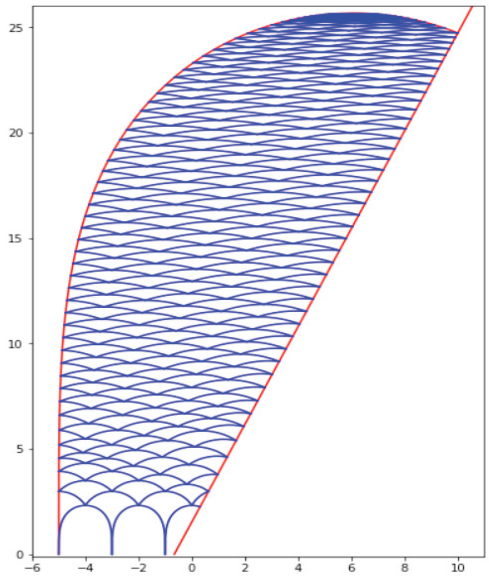

Fig. 3. (color online) Surface growth scheme in AdS_5 spacetime with a boundary, $\theta=\frac{\pi}{4}$ and $L=1$. The subregion A is divided into three subintervals, the left two include $\Delta x_1=2$ and the rest one has $\Delta x_1=0.18$. There are three types of starting/ending points for the growth of bulk extremal surfaces, one is on the bulk extremal surface of the subregion A, namely, the red RT surface, one is the turning point z_*, and the rest is a new one on the boundary Q. The number of growing layers correspond to 50.

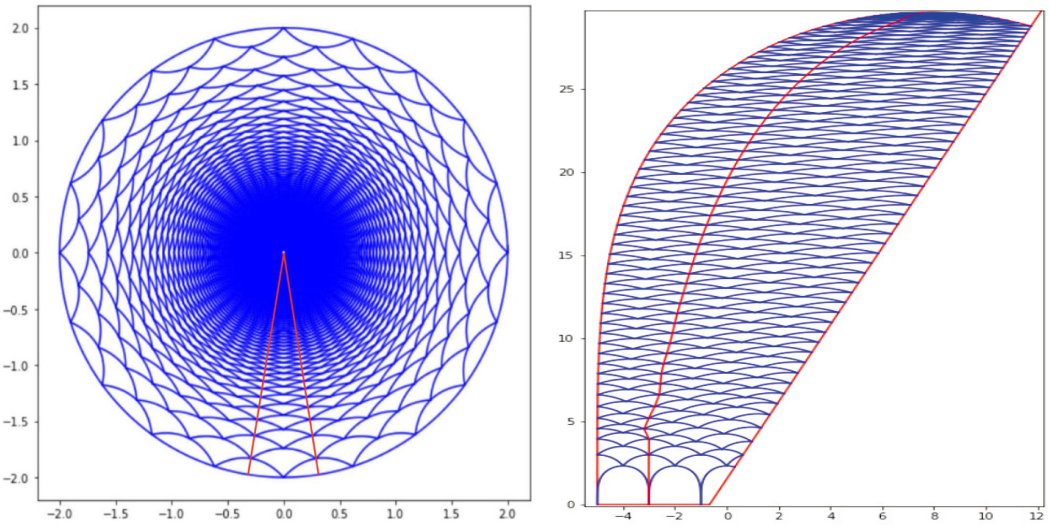

Fig. 4. (color online) Surface growth of strip-like bulk extremal surfaces in AdS spacetimes with and without boundary effects, and distinct properties of growing areas are shown. Left: The region between the two red curves represents a series of growing surfaces, with the boundary subregions partitioned equally. The areas of each layer decrease monotonically. The bulk spacetime is AdS_3 with $L=1$. Right: The region between the left two red curves (surfaces) represents a series of growing surfaces, and areas of each layer do not exhibit a strictly decreasing trend when going into the bulk AdS spacetime with boundary. The bulk spacetime is AdS_5 with $L=1$.

surfaces within layers in the surface growth scheme.

Furthermore, we also consider the surface growth in the case where the boundary subregions exhibit inhomogenous size. As illustrated in Fig. 5, in a manner similar to the case of surface growth without boundary, although the growing surfaces are inhomogeneous initially, the configuration becomes close to the homogenous case with a sufficient number of growth layers.

IV. RELATION BETWEEN THE SURFACE GROWTH SCHEME AND DEFECT MERA

In the previous section, we successfully extended the surface growth scheme into the AdS spacetime with a boundary, namely, the translational symmetry is broken at the boundary. It is observed that a set of strip-like bulk extremal surfaces can fill the entanglement wedge of a given boundary subregion layer-by-layer, and two distinct types of extremal surfaces will emerge during the surface growth process. A comparative analysis is performed between surface growth scheme with and without a boundary. On the other hand, we recall that in the absence of boundary, the surface growth scheme can correspond to the MERA-like tensor network [26], and thus it is natural to examine whether the surface growth scheme in AdS/BCFT duality can still correspond to some tensor network. To address this question, we note that from the geometric picture of the MERA, the surface growth scheme in AdS/BCFT duality is expected to correspond a MERA with boundary. This can be termed as the defect MERA [37].

The minimal updates method can be used to generalize the MERA of tensor network with boundary and especially its holographic duality [38, 39]. The main idea of minimal updates is that the initial system can naturally evolve into the defect system by modifying a segment of its inner structure located within the causal cone associated with defect or boundary in the lattice. We assume that H denotes the Hamiltonian of a homogeneous many-body quantum state, and $H^{\#}$ denotes the system with any defect, then

$$H^{\#} = H + H_d, \tag{9}$$

where H_d denotes the interaction term associated with a defect or boundary. With this Hamiltonian, the quantum state description of MERA undergoes corresponding changes to accommodate to the defect MERA, denoted as wave functions $|\varphi\rangle^{\#}$ and $|\varphi\rangle$, respectively. Subsequently, the causal cone of the defect can be defined via a consistent coarse-graining process.

We consider a one dimensional critical quantum system, in which the homogeneous Hamiltonian is $H=\sum_{r=-\infty}^{\infty} h(r,r+1)$, with a constant coupling constant h. The MERA of the system contains a pair of tensors $\{u,v\}$, where u denotes the disentangeler and v denotes the coarse-grainer. Based on minimal updates, the defect MERA of the quantum state with scale invariance manifests two pairs of tensors, denoted as $\{u,v\}$ and $\{u',v'\}$, representing regions outside and inside the causal cone $C(0)$ of the defect or boundary D, respectively. We then combine the surface growth approach in [26] and the method of minimal updates [38, 39]. Hence, it is reason-

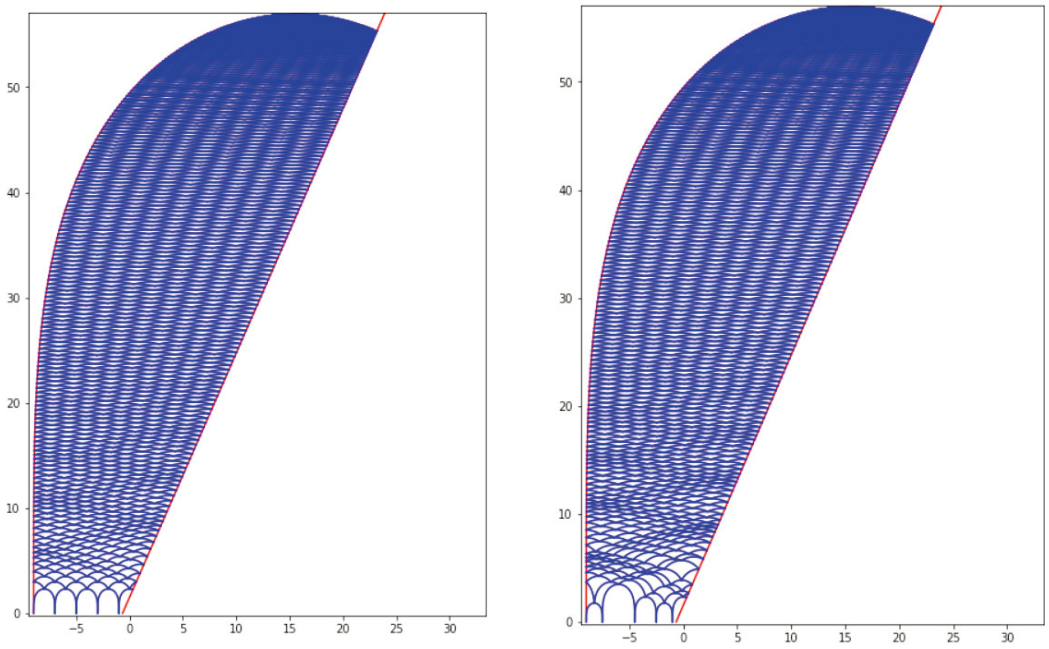

Fig. 5. (color online) Comparison of surface growth of strip-like bulk extremal surfaces between homogenous (Left) and inhomogenous (Right) boundary subintervals in $AdS_5/BCFT_4$ with $\theta=\frac{\pi}{3}$ and $L=1$. The subregion A is divided into five subintervals. Left: The surface growth of homogenous subintervals, the left four subintervals include $\Delta x_1=2$, the rest one include $\Delta x_1=0.18$, and number of growing layers is 500. Right: The surface growth for boundary subregions with inhomogenous subintervals, and the growing layers are also 500.

able to identify the surface growth configuration γ and $\bar{\gamma}$ with tensor pairs $\{u,v\}$ and $\{u',v'\}$, as shown in Fig. 6, in which $\{u',v'\}\Leftrightarrow\bar{\gamma}$ and $\{u,v\}\Leftrightarrow\gamma$.

More explicitly, the state of the BCFT can be represented as a product of holographic tensor network state, i.e., the distilled maximal entanglement state

$$\begin{aligned}|\Psi\rangle &= W^{A}_{1\beta\bar{\alpha}}W^{\bar{A}}_{2\bar{\beta}\alpha}\phi^{\alpha\bar{\alpha}}\sigma^{\beta\bar{\beta}}\\ &= (W_1\otimes W_2)(|\phi\rangle\otimes|\sigma\rangle)\otimes\left(W_1'\otimes W_2'\right)(|\phi'\rangle\otimes|\sigma'\rangle),\end{aligned}\tag{10}$$

where W_1 and W_2 denote the isometry tensors which map the states $|\phi\rangle$ and $|\sigma\rangle$ into the reduced density matrix of boundary subregion A and its complement $\bar{A}$, respectively. $|\phi\rangle$ denotes the dominant state and $|\sigma\rangle$ denotes the quantum fluctuation. While W', $|\phi'\rangle$ and $|\sigma'\rangle$ denote their counterparts within the causal cone $C(0)$. By repeating the above entanglement distillation procedure, the OSED defect tensor network corresponding to the surface growth with boundary can be constructed as in Fig. 6. This provides a specific form of bulk reconstruction from surface growth in the AdS/BCFT correspondence.

V. ENTANGLEMENT OF PURIFICATION IN SURFACE GROWTH SCHEME

The surface growth process can divide the entanglement wedge into arbitrary subregions, which is expected to capture the fine structure of the entanglement entropy in these subregions such as the entanglement contour [40, 41]. Additionally, it was shown in [42] that the holographic duality of the entanglement purification [43, 44] can also be derived from a specific surface growth scheme. Therefore, it is interesting to further investigate the entanglement of purification in surface growth scheme in the AdS/BCFT correspondence. The holographic duality of entanglement of purification is given by the entanglement wedge cross section Σ_{AB} as [45, 46]

$$E_P(\rho_{AB})=\min\left[\frac{\text{Area}(\Sigma_{AB})}{4G_N}\right],\tag{11}$$

where A and B denote two boundary disjoint subsystems, the entanglement wedge W are bounded by extremal surfaces of A and B, and the connected extremal surfaces Σ_A and Σ_B of region $A\cup B$.

We consider a BCFT case in AdS_3 spacetime as shown in Fig. 7, the subregion A and a boundary region p_0P share a entanglement wedge, the entanglement wedge cross section p_0p_1 is defined as the surface between the endpoints of boundary p_0 and RT surface γ_0. To describe the entanglement of purification, p_0p_1 should correspond to a minimal surface (namely, a geodesic). We note that the formula of geodesic distance D between two spacetime points (t_1,x_1,z_1) and (t_2,x_2,z_2) in AdS_3 spacetime in Poincaré coordinate is:

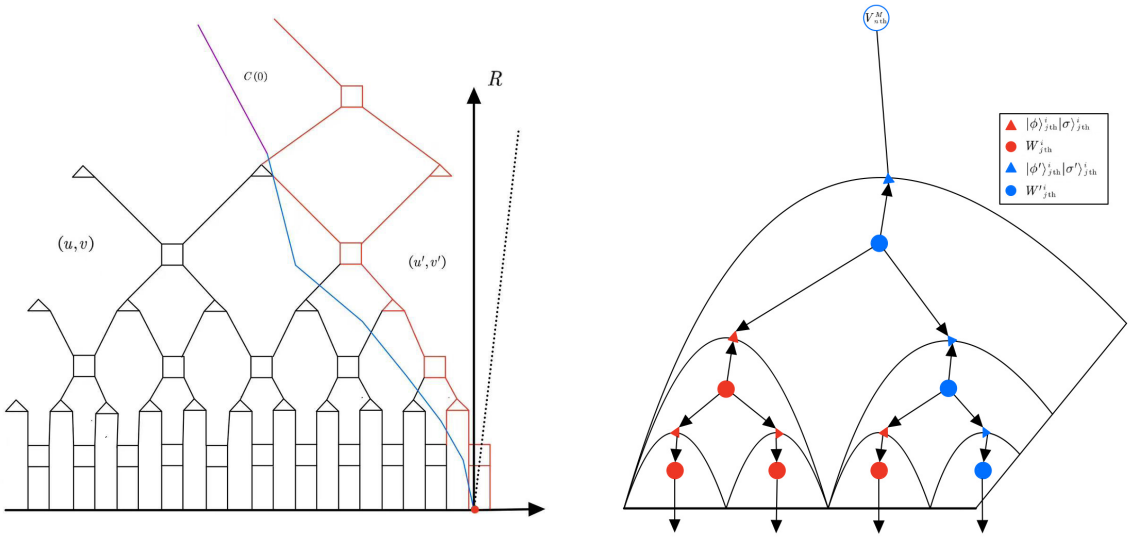

Fig. 6. (color online) Structure of defect MERA and product OSED process. Left: blue line denotes the boundary of the casual cone $C(0)$ associated with the defect or boundary in the lattice, R denotes the direction of renormalization. The red square and triangle and their blue counterparts denote the disentangler and coarse graining tensors inside and outside the causal cone respectively. Right: given the boundary effect, the modified OSED tensor network contains two representation of approximate quantum state production, corresponding to the boundary surface growth scheme.

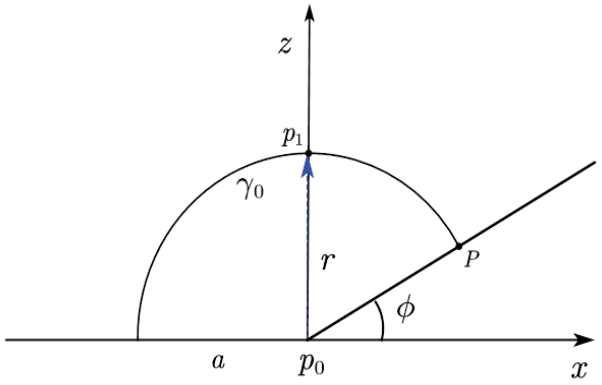

Fig. 7. (color online) Entanglement wedge cross section of subregion A (with length a) and boundary region p_0P of a BCFT in AdS_3 spacetime. The blue arrow denotes the position of the entanglement wedge cross section p_0p_1, which connects the boundary point p_0 and the bulk RT surface, and $\phi=\frac{\pi}{6}$. The holographic description of the entanglement of purification corresponds to p_0p_1 when it is a minimal surface.

$$\cosh\frac{D}{L}=\left|1+\frac{-(t_1-t_2)^2+(x_1-x_2)^2+(z_1-z_2)^2}{2z_1z_2}\right|, \tag{12}$$

and the static geodesic (namely, $t_1=t_2$) satisfies the equation of a circle, *i.e.*, $(x-x_c)^2+(z-z_c)^2=r^2$ (where (x_c,z_c) is the location of the center and r denotes the radius of the circle, respectively). In Fig. 7, the angle between p_0p_1 and p_0P is set as θ, the radius of the geodesic circle is r, and the coordinate p_0 on the asymptotically AdS_3 boundary is $(0,\epsilon)$. Then, from Eq. (12), if the static geodesic distance between p_0 and p_1 satisfies

$$\cosh\frac{D_{p_0p_1}}{L}=1+\frac{r^2\cos^2(\theta+\phi)+(r\sin(\theta+\phi)-\epsilon)^2}{2\epsilon r\sin(\theta+\phi)}, \tag{13}$$

then $\frac{\mathrm{d}}{\mathrm{d}\theta}\cosh\frac{D_{p_0p_1}}{L}=0$ provides $\cos(\theta+\phi)=0$, *i.e.* $\theta+\phi=\frac{\pi}{2}$, namely, the entanglement of purification corresponds to the case in which p_0p_1 is perpendicular to x axis.

We then focus on studying the entanglement of purification in a specific surface growth configurations in the $AdS_3/BCFT_2$ correspondence via investigating the entanglement wedge cross section at each step of the surface growth process. The specific surface growth configuration consists of extremal surfaces which end on the previous one and the boundary, and the entanglement of purification are geodesics between the point p_i and the next layer extremal surface γ_i. It is noted that in the process of surface growth, the starting and ending points of the next layers depend on various conditions such as the size and symmetry of the previous layers and the boundary condition. Given the entanglement of purification is a minimal surface which contains minimal entanglement entropy from the BCFT side, we suggest that it can serve as a selection rule to chose the starting point of the growing minimal surfaces.

For the two layers surface growth case, as shown in Fig. 8, the closed surface $p_1P_1P_2p_2$ can be holographically interpreted as a pure state from the surface/state correspondence [47], we then select the geodesic curve p_1P_1 and the region P_1P_2 as the subsystems in the bulk and on the boundary, respectively, the entanglement of purification in the second layer corresponds to minimize the en-

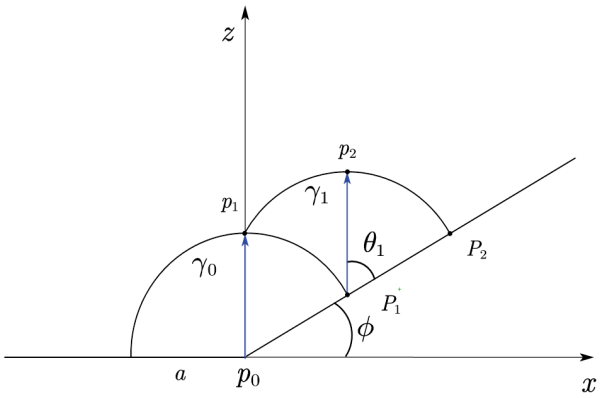

Fig. 8. (color online) Entanglement wedge cross section in the second layer of growing minimal surface, the boundary angle is $\phi = \frac{\pi}{6}$, γ_0 and γ_1 denote the first and second layer extremal surfaces, respectively. The blue arrow denotes the geodesic between two surface, θ_1 denotes the angle between the entanglement wedge cross section P_1p_2 and the boundary.

tanglement wedge cross section P_1p_2, and the angle θ_1 will be determined in the following multi-layers surface growth configuration.

In the surface growth process, from the second layer on, each layer of the extremal surface starts at the point p_i of the previous layer, thereby indicating that each surface intersects both the boundary and the previous entanglement wedge cross section. Subsequently, the entanglement of purification in the next layer also follows the surface growth scheme and be calculated by determining the minimal surface between the point p_i and the next extremal surface γ_{i+1}. More explicitly, the ending point P_i of the i-th extremal surface on the boundary naturally serves as the new boundary of the spacetime, we can select location of P_i to be (m_i, n_i), the angle between the entanglement wedge cross section P_ip_{i+1} with the boundary is θ_i, and the radius of the geodesic circle γ_i to be r_i. We then use Eq. (12), and the geodesic distance $D_{P_ip_{i+1}}$ between the boundary point P_i and the intersection point p_{i+1} on the extremal surface γ_i satisfies

$$\cosh\frac{D_{P_ip_{i+1}}}{L} = 1 + \frac{(r_i\cos(\theta_i+\phi))^2 + (r_i\sin(\theta_i+\phi))^2}{2n_i(n_i + r_i\sin(\theta_i+\phi))}. \quad (14)$$

Subsequently, $\frac{\mathrm{d}}{\mathrm{d}\theta_i}D_{P_ip_{i+1}} = 0$ also gives $\theta_i + \phi = \frac{\pi}{2}$.

We can obtain a homogenous surface growth configuration in this case by selecting $\phi = \pi/6$, then each geodesic circle exhibits the same radius $r = a$. We then iterate this process to obtain any number of layers of surface growth, for example, Fig. 9 illustrates the entanglement of purification in seven layers of homogenous surface growth. Furthermore, it is straightforward to see that when $\phi > \pi/6$, the surface growth configurations are not homogenous and will decay after finite steps of surface growth. Given that the entanglement of purification contains the minimal entanglement entropy in a given entanglement wedge, the intersection point p_i naturally yields a fixed point and serves as the starting point of the next layer of growing surface, which gives more refined description of entanglement entropy in the entanglement

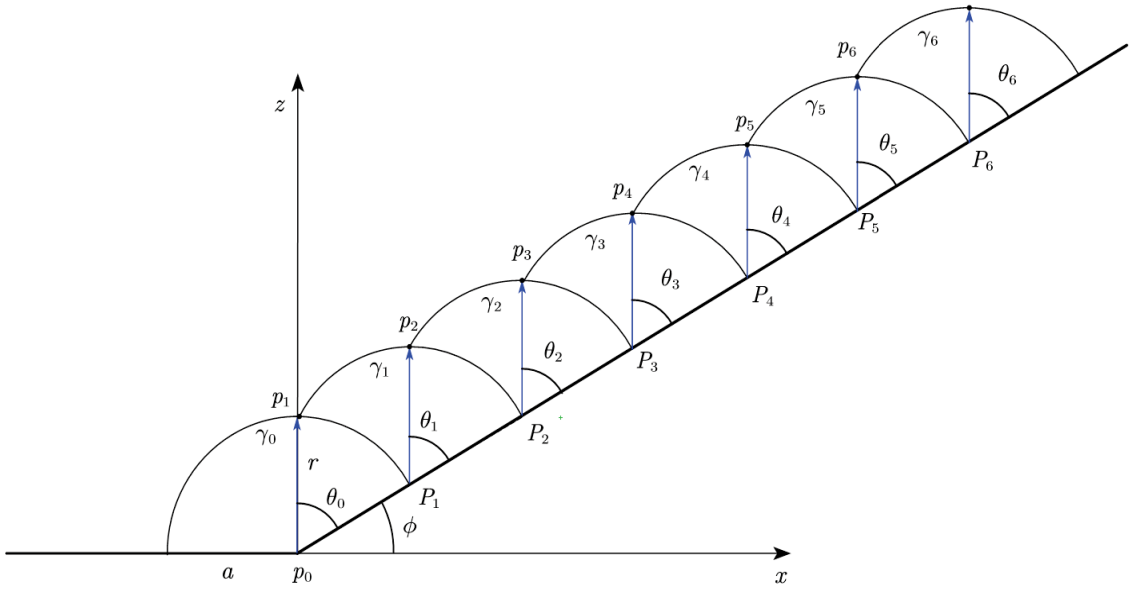

Fig. 9. (color online) Entanglement wedge cross section in the surface growth scheme which contains seven layers of growing surfaces, γ_i denotes the extremal surface in the $i+1$-th layer, θ_i denotes the location of wedge cross-section which are all equal to $\pi/3$ and the boundary angle is $\phi = \pi/6$. The blue arrows denote the geodesics and indicate the direction of the entanglement of purification, and note that each geodesic circle has the same radius $r = a$.

wedge and indicates that the entanglement of purification affects the dynamics of the surface growth for bulk reconstruction in the AdS/BCFT correspondence.

VI. CONCLUSION AND DISCUSSION

In the study, we extend the surface growth approach for bulk reconstruction into the AdS/BCFT correspondence. Our investigation mainly focus on the growth of strip-like bulk extremal surfaces in the presence of an additional spatial boundary, we show that the outer entanglement wedge can be constructed from the growth of two types of extremal surfaces, namely, the type which will attach the boundary and the other typre which will not, layer by layer in both the homogenous and inhomogenous boundary subsystems.

In addition, we also show that the surface growth process in BCFT can correspond to the defect MERA tensor network by generalizing OSED tensor network into the situation with boundary or defect, which further demonstrates the connection between the emergence of bulk geometry and entanglement renormalization of the tensor networks. Furthermore, the surface growth scheme can divide a given entanglement wedge into arbitrary subregions, which naturally captures the fine structure of the entanglement entropy and reflects the correlations between these subregions. Thus, we examine the entanglement of purification by investigating the entanglement wedge cross section in the surface growth scheme in AdS_3 spacetime with boundary. Furthermore, we demonstrate that entanglement of purification can be determined in each step of the surface growth and can serve as a selection rule for the starting point of the next layer of extremal surface. This provides a more refined description of the entanglement entropy in the entanglement wedge and can also affect the dynamics in the surface growth scheme for bulk reconstruction.

Many intriguing avenues for further research exist, such as expanding the surface growth scheme to boundary CFTs with more complex defect conditions or multiple boundaries. In these cases, each defect, represented by a defect tensor network, includes its own causal wedge that influences the surface growth process. Additionally, it is important to examine the surface growth scheme in higher dimensional BCFT case and the BCFT whose bulk duality contains a black hole.

ACKNOWLEDGEMENT

We are grateful to L.-Y. Hung for useful discussions.

References

[1] J. M. Maldacena, Adv. Theor. Math. Phys. **2**, 231 (1998)
[2] S. S. Gubser, I. R. Klebanov, and A. M. Polyakov, Phys. Lett. B **428**, 105 (1998), arXiv:hep-th/9802109]
[3] E. Witten, Adv. Theor. Math. Phys. **2**, 253 (1998), arXiv:hep-th/9802150]
[4] S. Ryu and T. Takayanagi, Phys. Rev. Lett. **96**, 181602 (2006), arXiv:hep-th/0603001
[5] S. Ryu and T. Takayanagi, JHEP **0608**, 045 (2006), arXiv:hep-th/0605073
[6] V. E. Hubeny, M. Rangamani, and T. Takayanagi, JHEP **0707**, 062 (2007), arXiv:0705.0016[hep-th]
[7] M. Rangamani and T. Takayanagi, *Holographic Entanglement Entropy*, Lect. Notes Phys. **931** (Springer, 2017), pp.1-246
[8] T. Faulkner and A. Lewkowycz, JHEP **07**, 151 (2017), arXiv:1704.05464[hep-th]
[9] N. Bao, C. Cao, S. Fischetti *et al.*, Class. Quant. Grav. **36**(18), 185002 (2019), arXiv:1904.04834
[10] S. R. Roy and D. Sarkar, Phys. Rev. D **98**(6), 066017 (2018), arXiv:1801.07280
[11] X. Dong, D. Harlow, and A. C. Wall, Phys. Rev. Lett. **117**(2), 021601 (2016), arXiv:1601.05416[hep-th]
[12] J. Cotler, P. Hayden, G. Penington *et al.*, Phys. Rev. **X9**(3), 031011 (2019), arXiv:1704.05839[hep-th]
[13] G. Vidal, Phys. Rev. Lett. **101**, 110501 (2008), arXiv:quant-ph/0610099
[14] B. Swingle, Phys. Rev. D **86**, 065007 (2012), arXiv:0905.1317[cond-mat.str-el]
[15] G. Vidal, Phys. Rev. Let. **99**, 220405 (2007)
[16] A. Milsted and G. Vidal, arXiv: 1812.00529
[17] N. Bao, G. Penington, J. Sorce *et al.*, JHEP **19**, 069 (2020), arXiv:1812.01171[hep-th]
[18] L. Y. Hung, W. Li, and C. M. Melby-Thompson, JHEP **04**, 170 (2019), arXiv:1902.01411[hep-th]
[19] P. Hayden, S. Nezami, X. L. Qi *et al.*, JHEP **11**, 009 (2016), arXiv:1601.01694[hep-th]
[20] R. Vasseur, A. C. Potter, Y. Z. You *et al.*, Phys. Rev. B **100**(13), 134203 (2019), arXiv:1807.07082[cond-mat.stat-mech]
[21] T. Faulkner, M. Li, and H. Wang, JHEP **04**, 119 (2019), arXiv:1806.10560
[22] A. Almheiri, X. Dong, and D. Harlow, JHEP **04**, 163 (2015), arXiv:1411.7041[hep-th]
[23] G. Penington, JHEP **09**, 002 (2020), arXiv:1905.08255[hep-th]
[24] F. Pastawski, B. Yoshida, D. Harlow *et al.*, JHEP **06**, 149 (2015), arXiv:1503.06237[hep-th]
[25] H. Y. Dai, J. R. Sun, and Y. Sun, Commun. Theor. Phys. **75**(8), 085402 (2023), arXiv:1912.02070[hep-th]
[26] Y. Y. Lin, J. R. Sun, and Y. Sun, JHEP **12**, 083 (2020)
[27] C. Yu, F. Z. Chen, Y. Y. Lin *et al.*, Chin. Phys. C **46**(8), 085104 (2022), arXiv:2010.03167[hep-th]
[28] M. Fujita, T. Takayanagi, and E. Tonni, JHEP **11**, 043 (2011), arXiv:1108.5152[hep-th]
[29] T. Takayanagi, Phys. Rev. Lett. **107**, 101602 (2011), arXiv:1105.5165[hep-th]
[30] J. L. Cardy, arXiv: hep-th/0411189[hep-th]
[31] C. S. Chu, R. X. Miao, and W. Z. Guo, JHEP **04**, 089 (2017), arXiv:1701.07202[hep-th]
[32] A. Almheiri, R. Mahajan, J. Maldacena *et al.*, JHEP **03**, 149 (2020), arXiv:1908.10996[hep-th]

[33] H. Z. Chen, R. C. Myers, D. Neuenfeld *et al*., JHEP **10**, 166 (2020), arXiv:2006.04851[hep-th]
[34] H. Z. Chen, R. C. Myers, D. Neuenfeld *et al*., JHEP **12**, 025 (2020), arXiv:2010.00018[hep-th]
[35] Y. Y. Lin, J. R. Sun, Y. Sun *et al*., JHEP **07**, 009 (2022), arXiv:2203.03111[hep-th]
[36] R. X. Miao, JHEP **03**, 214 (2023), arXiv:2301.06285[hep-th]
[37] G. Evenbly, R. N. C. Pfeifer, V. Pico *et al*., Phys. Rev. B **82**, 161107(R) (2010), arXiv:0912.1642[cond-mat.str-el]
[38] B. Czech, P. H. Nguyen, and S. Swaminathan, JHEP **03**, 090 (2017), arXiv:1612.05698[hep-th]
[39] G. Evenbly and G. Vidal, Phys. Rev. B **91**, 205119 (2015), arXiv:1307.0831[quant-ph]
[40] G. Vidal and Y. Chen, J. Stat. Mech. **2014**(10), P10011 (2014), arXiv:1406.1471[cond-mat.str-el]
[41] L. H. Mo, Y. Zhou, J. R. Sun *et al*., arXiv:2311.01997[quant-ph]
[42] Y. Y. Lin, J. R. Sun, and Y. Sun, Phys. Rev. D **103**(12), 126002 (2021), arXiv:2012.05737[hep-th]
[43] T. Takayanagi and K. Umemoto, Nature Phys. **14**(6), 573 (2018), arXiv:1708.09393[hep-th]
[44] P. Nguyen, T. Devakul, M. G. Halbasch *et al*., JHEP **01**, 098 (2018), arXiv:1709.07424[hep-th]
[45] B. Czech, J. L. Karczmarek, F. Nogueira *et al*., Class. Quant. Grav. **29**, 155009 (2012), arXiv:1204.1330[hep-th]
[46] D. L. Jafferis, A. Lewkowycz, J. Maldacena *et al*., JHEP **06**, 004 (2016), arXiv:1512.06431[hep-th]
[47] M. Miyaji and T. Takayanagi, Prog. Theor. Exp. Phys. **2015**, 073B03 (2015), arXiv:1503.03542[hep-th]